Temperature and Thermal Stress Distributions in a Tubular Solid Oxide Fuel Cell

Kiyoshi KANAMURA* and Zen-ichiro TAKEHARA
Division of Energy and Hydrocarbon Chemistry, Graduate School of Engineering, Kyoto University, Yoshida-honmachi, Sakyo-ku, Kyoto 606-01

(Received February 18, 1993)

The temperature and thermal stress distributions in two model cells for a tubular solid oxide fuel cell, which have a different thickness of the electrolyte, were calculated by the finite element method to demonstrate the effects of electrolyte thickness on the mechanical stability of fuel cells. When the cells were operated at a constant voltage, their energy conversion efficiency increased with decreasing thickness of the electrolyte. A larger amount of heat was generated in the cell having a thinner electrolyte, thus producing a larger thermal stress. These results indicates that an excellent preparation method for the highly ionic conductive electrolyte is essential to produce a fuel cell with high mechanical stability.

Solid oxide fuel cells (SOFCs) have been investigated to produce electric energy from various kinds of fuels with a high energy conversion efficiency. The mechanical stability of materials consisting of SOFCs is the most important problem to make SOFCs practical. Various kinds of compounds have been proposed as materials for electrolyte, cathode, anode, and substrate.[1—3] The SOFCs have to be operated around 1273 K, because the most of the solid oxide electrolytes show ionic conductivities high enough for practical use at this temperature. Thermal expansion takes place during the operation of SOFCs at a high temperature (1273 K). The analysis of thermal expansion of cell materials is necessary for SOFC design. However, the thermal expansion of each material in SOFC cannot be measured directly. Some researchers have calculated the temperature distribution in SOFCs.[4,5] It is related to the mechanical stability of SOFC, because the thermal stress is produced in the cell as a result of the temperature distribution. The thermal stress is also related to the mechanical properties and dimensions of cell materials.

In this study, the calculation of the thermal stress distribution in the tubular SOFC was conducted by the finite element method to demonstrate the effects of the thickness of the electrolyte on the mechanical stability and the electrochemical characteristics of the cell.

Calculation of Temperature Distribution

Figure 1 shows model cells for the tubular SOFCs, which are much smaller than a practical cell. The thickness of each element is summarized in Table 1. The cell length assumed was 40 mm and the inside diameter 5.2 mm. Two kinds of SOFCs, which have a different thickness of electrolyte, were adopted as model cells in this study. In both cells, porous yttria-stabilized zirconia, porous $LaMnO_3$, compact yttria-stabilized zirconia, and nickel-yttria-stabilized zirconia cermet were used as substrate, cathode, electrolyte, and anode, respectively. The thickness of porous substrate, porous cathode, and porous anode in model cell 2 were same with those in model cell 1. The thickness of electrolyte in model cell 2 was assumed to be five times as large as

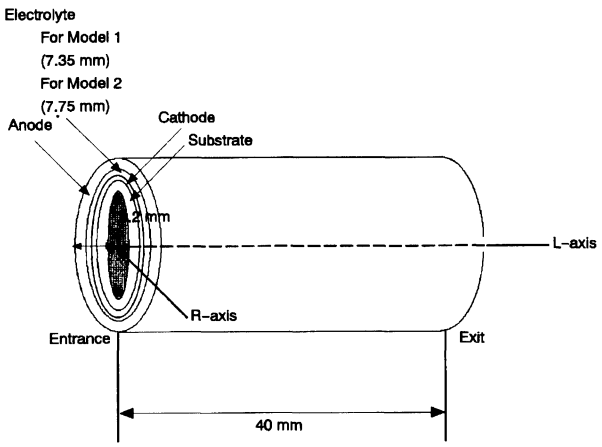

Fig. 1. Schematic illustration of model cell for the tubular solid oxide fuel cells.

that in model cell 1. The thermal stress distribution in the tubular SOFC can be calculated from the temperature distribution using the finite element method. The calculation of temperature distribution can be done using the finite element method. Before the calculation of temperature distribution, the amount of heat generation and absorption at each part of the model cell must be estimated.

Assuming that the cell is discharged at constant voltage, 0.8 V, the heat generation and absorption in the model cell can be calculated. The temperature of the model cell at the initial state was assumed to be 1273 K. The partial pressures of oxygen, hydrogen, and steam at the entrance of cathode or anode chambers were assumed to be 0.21, 0.95, and 0.05 atm, respectively (see Fig. 8). The flow rates of air and fuel were assumed to be 20 and 5 cm s^{-1}, respectively. The conductivities of porous anode and cathode are assumed to be so high that the voltage drop in these electrodes along the L-axis can be neglected. The relationship between current and voltage was approximated by the following empirical equations, which were obtained from the modification of the current–voltage curves for practical large cell,[6]

$$V = V_0 - (I \times (R_1 + R_2) + 0.15) \quad (1)$$

$$R_1 = \frac{0.85(\Omega\ \mathrm{cm}^2)}{2 \times \pi \times r_1 \times L_e}(\Omega) \quad (2)$$

$$R_2 = \frac{10(\Omega\ \mathrm{cm}) \times l}{2 \times \pi \times r_2 \times L_e}(\Omega) \quad (3)$$

where V is the cell voltage (0.8 V), V_0 is the open circuit voltage, I is the current, R_1 is the resistance due to the overpotential of the anode reaction, R_2 is the resistance of the electrolyte along the R axis, and r_1 and r_2 are the average radius of anode and electrolyte, respectively. l is the thickness of electrolyte and L_e is the length of the cell element (L_e=2 mm). The polarizations for cathode reaction in both model cells are neglected.[7] 0.15 in Eq. 1 is the adjustment parameter to fit the approximated linear current–voltage relationship to the practical one. The current distribution was calculated assuming the equivalent circuit as shown in Fig. 2, according to a reference reported previously.[8] In this study, the resistance of electrodes along the L-axis was neglected. These resistances become more important for the longer cells (for example a 100-cm length cell).

Figure 3 shows the current distributions in two model cells along the L-axis. The current in model cell 1 was larger than that in model cell 2. The ohmic resistance of electrolyte in model cell 1 is smaller than that in the model cell 2. The resistance for anode reaction in model cell 1 is larger than that in model cell 2, because the electrode area of model cell 1 is smaller than that of model cell 2. The higher current in model cell 1 indicates that the contribution of the ohmic resistance of electrolyte on total polarization for cell reaction is larger than any other factors. Thus model cell 1 had the larger electric energy than model cell 2. The energy conversion efficiency increased with decreasing thickness of electrolyte.

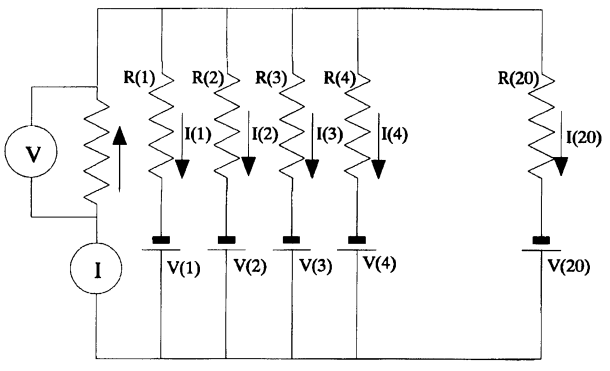

I(n) : Current for nth element
R(n) : Total resistance for nth element
V(n) : Voltage for nth element
V=V(1)=V(2)=V(3) ----- =V(20)
I=I(1)+I(2)+I(3)+ ----- +I(20)

Fig. 2. Equivalent circuit for the model SOFC.

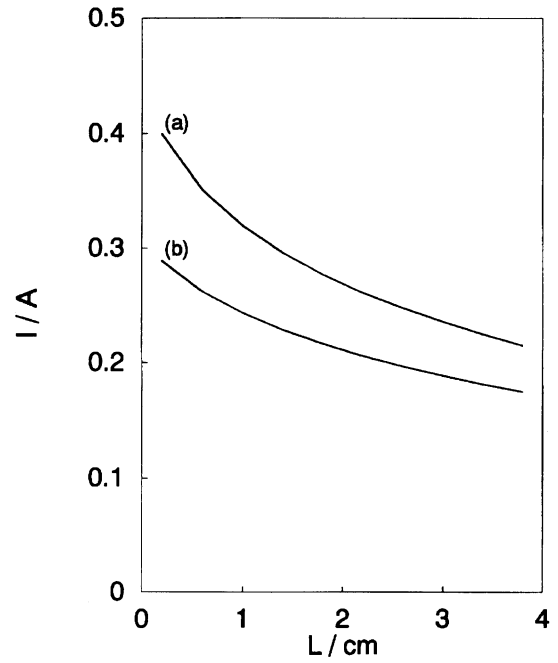

Fig. 3. Current distributions along the L-axis in the tubular solid oxide fuel cells, (a) : model 1, (b) : model 2.

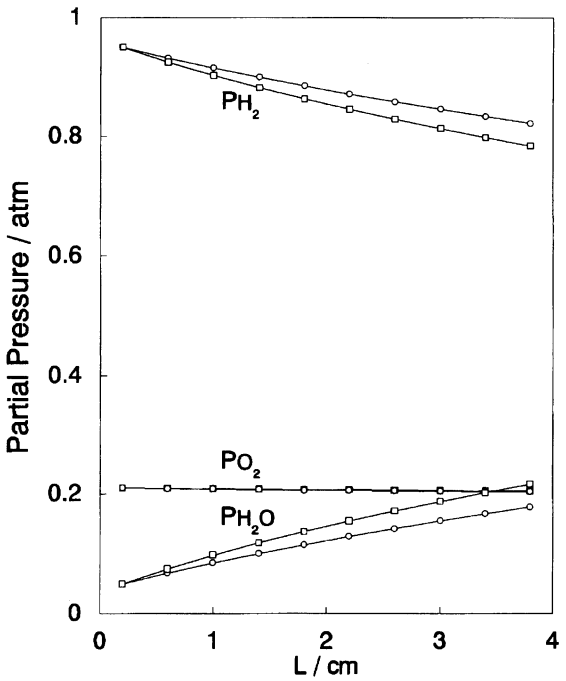

Fig. 4. Partial pressure distributions along the L-axis in the tubular solid oxide fuel cells, ○ : model 1, □ : model 2.

Figure 4 shows the partial pressure distributions of hydrogen, steam, and oxygen in two model cells. The partial pressures of hydrogen, oxygen, and steam depend on the current distribution. The decrease in the hydrogen partial pressure was much larger than that in oxygen partial pressure. This is caused by the differ-

Table 1. Dimensions of Each Part of Model Cells

Part	Thickness	
	(For model cell 1)	(For model cell 2)
Porous substrate (Yttria-stabilized zirconia)	1.25 mm	1.25 mm
Porous cathode ($LaMnO_3$)	0.70 mm	0.70 mm
Electrolyte (Yttria-stabilized zirconia)	0.10 mm	0.50 mm
Porous anode (Ni-zirconia cermet)	0.10 mm	0.10 mm

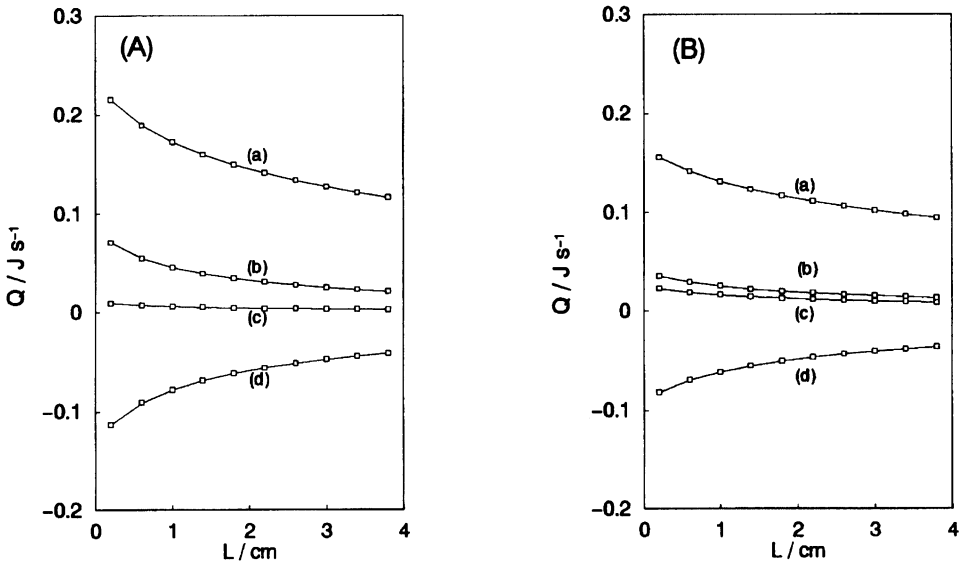

Fig. 5. Heat generation and absorption in the tubular solid oxide fuel cells (a) : heat generation from the entropy change for the cathode reaction, (b) : heat generation from the ohmic resistance of electrolyte, (c) : heat generation from the overpotential for the anode reaction, (d) : heat absorption by the entropy change for the anode reaction, (A) : for model cell 1, (B) : for model cell 2.

ences in the flow rate of these gasses and the electrochemical reaction order. The use of hydrogen in model cell 1 was 18% and was larger than that in model cell 2.

From the current distribution, the heat generation and absorption in the cell were estimated. The heat boundary exists at the interface between fuel gas and anode or air and substrate. The heat transfer coefficient strongly depend on the cell design, especially the shape of the gas distributor. In this study, the heat transfer coefficients at these interfaces were assumed to be 30 mJ K^{-1} cm^{-2}. The heat transport was calculated from the temperature difference between gas and electrode. The heat was generated or absorbed by the ohmic resistance of electrolyte, the overpotentials for cathode and anode reactions, and the entropy changes for the cathode and anode reactions. In this calculation, the cathode overpotential was assumed to be negligibly small.[7] The entropy changes for cathode and anode reactions were estimated from the Seebeck coefficients for cathode and anode reactions.[9,10] The entropy change for cathode or anode reaction depends on the partial pressures of hydrogen and steam, or oxygen, respectively. In this study, the dependence of the entropy change for the cathode reaction on the partial pressure of oxygen was neglected, because the partial pressure of oxygen did not change significantly under these operating conditions, as shown in Fig. 4. The dependence of the entropy change for the anode reaction on the partial pressure was taken into account for the calculation of the temperature distribution. The amount of heat generated and absorbed by these factors were related to the current distribution, as follows,

$$\text{Cathode} : Q = I \times T \times \Delta S_c, \tag{4}$$

$$\text{Anode} : Q = I \times T \times \Delta S_a + I^2 \times R_1, \tag{5}$$

$$\text{Electrolyte} : Q = I^2 \times R_2, \tag{6}$$

where Q is the amount of heat per second, ΔS_c is the entropy change for the cathode reaction and assumed to be 56.7 kJ mol^{-1} K^{-1}, ΔS_a is the entropy change for

anode reaction and is estimated from the value of ΔS_c and the following equation, where the total pressure of hydrogen and steam was assumed to be 1.

$$\Delta S_a = (S^0_{H_2O} - S^0_{H_2} - \frac{1}{2} \times S^0_{O_2}) - R \ln \frac{1 - P_{H_2}}{P_{H_2} \times 0.21^{\frac{1}{2}}} - \Delta S_c \quad (7)$$

Figure 5 shows the distribution of heat generation or absorption in the cell caused by various factors. The amount of heat generated or absorbed in model cell 1 was larger than that in model cell 2, as seen from the current distributions in these cells. In both cells, the largest heat generation was caused by the entropy change for cathode reaction. The heat was absorbed by the entropy change for the anode reaction. These results indicate that the entropy changes for the electrode reactions strongly influence the temperature distribution in the solid oxide fuel cell. It is interesting to note that the entropy change for electrode reaction cannot be reduced, because that is a thermodynamic phenomenon. On the other hand, the heat generation caused by the polarization of the anode reaction and the ohmic resistance of electrolyte will be reduced by the improvement of anode material and the reduction of electrolyte thickness. With progress in the cell materials, the heat generation or absorption caused by the entropy change for the electrode reaction will become more important.

The thermal parameters of cell materials were summarized in Table 2.[2] The thermal conductivities of porous $LaMnO_3$and porous substrate were estimated from the average value of thermal conductivities calculated from series and parallel models using the following empirical equations.[11,12]

$$\text{For series} : \kappa = \nu_1\kappa_1 + \nu_2\kappa_2, \quad (8)$$

$$\text{For parallel} : \kappa = \frac{\kappa_1\kappa_2}{\nu_1\kappa_2 + \nu_2\kappa_1}, \quad (9)$$

where κ is the thermal conductivity of porous $LaMnO_3$ or porous substrate, κ_1 and κ_2 are the thermal conductivities of gas and solid phases, respectively. ν_1 and ν_2 are the volume ratios of gas and solid phases, respectively. The anode consists of a mixture of nickel and yttria-stabilized zirconia. To provide the high electric conductivity of the cermet electrode, the nickel matrix should be a continuum along the L-axis and R-axis. For such a material, the following empirical equation can be used,[11]

$$\kappa_m = \kappa_c \frac{1 + 2\nu_d(1 - \kappa_c/\kappa_d)/(2\kappa_c/\kappa_d + 1)}{1 - \nu_d(1 - \kappa_c/\kappa_d)/(\kappa_c/\kappa_d + 1)}, \quad (10)$$

Table 2. Heat Conductivities of Materials Consisting of the Tubular Solid Oxide Fuel Cells

Material	Heat conductivity/J s^{-1} cm^{-1} K^{-1}
YSZ	0.027
$LaMnO_3$	0.06
Ni	0.42

where ν_d is the volume ratio of yttria-stabilized zirconia, κ_d is the thermal conductivity of yttria-stabilized zirconia, κ_c is the thermal conductivity of nickel, κ_m is thermal conductivity of the mixed phase. The calculation of the temperature distribution was done by the finite element method.[8] The gas temperature increased during the operation of the cell. The amount of heat transferred through the heat boundary changed during the operation of the cell. In this calculation, the gas temperature in each element was calculated from the heat transfer coefficient and the temperature difference between the cell material and gas. Then the calculation of the temperature distribution using the finite element method was done again. This procedure was repeated until the amount of heat transferred though the heat boundary reached less than 1% of the initial value. Figures 6 and 7 show the temperature distributions along the R-axis near the entrance of two model cells and the Z-axis in the electrolyte, respectively. The temperature distribution between cathode and anode for model cell 1 (thickness of the electrolyte: 100 μm) was smaller than that for the model cell 2 (thickness of the electrolyte: 500 μm). This is caused by the higher heat transport in model cell 1, which is due to the thin electrolyte. Thus, the thickness of the electrolyte influences the temperature distribution along the R-axis. The highest temperature along the R-axis was observed at the cathode region in both cells. This result is due to the largest heat generation in the cathode region, especially due to the entropy change for the cathode reaction. On the other hand, the highest temperature along the Z-axis was observed at the entrance region. Such distributions correspond to the current distribution in the cells. The temperature distribution in model cell causes the thermal expansion of the cell materials. The stability of the cell is influenced by such an expansion.

Calculation of Thermal Stress Distribution

A schematic illustration for the boundary conditions in the calculation of thermal stress distribution is shown in Fig. 8. In this model, the cell was fixed by supports at the ends of the tube. The mechanical properties of cell materials are summarized in Table 3.[11] The mechanical properties of cell materials depend on their porosities. The effects of porosity on the modulus elasticity (E) of cell materials were evaluated using the following equation,[11]

$$E = E_0(1 - 1.9 \times P + 0.9 \times P^2) \quad (11)$$

where P is the porosity of the cell material. The calculation of the thermal stress distribution was done using the finite element method, where the temperature distributions shown in Figs. 6 and 7 were used.

Figure 9 shows the distributions of principal and shearing stresses in the model cell 1 along the Z-axis and R-axis. The principal stresses (σ_{RR} and σ_{ZZ}) cor-

Table 3. Mechanical Properties of Cell Materials

Material	Coefficient of linear expansion (K^{-1})	Modulus of elasticity ($g\ cm^{-2}$)	Poisson's ratio
YSZ	3.8×10^{-6}	1.55×10^{8}	0.25
Porous YSZ substrate	3.3×10^{-6}	7.91×10^{7}	0.25
Porous cathode	2.0×10^{-5}	7.08×10^{8}	0.25
Porous anode	1.7×10^{-5}	3.59×10^{7}	0.4

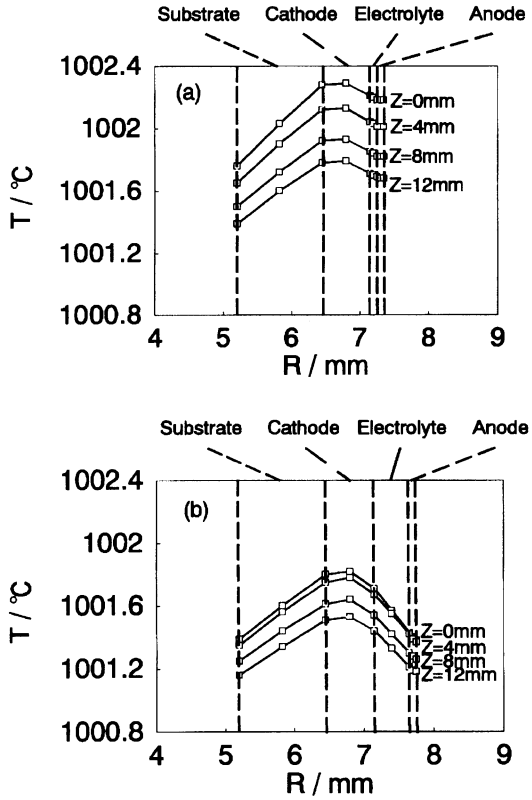

Fig. 6. Temperature distributions in the tubular solid oxide fuel cells along the R-axis, Z: distance from the entrance of the cell, (a): model cell 1, (b): model cell 2.

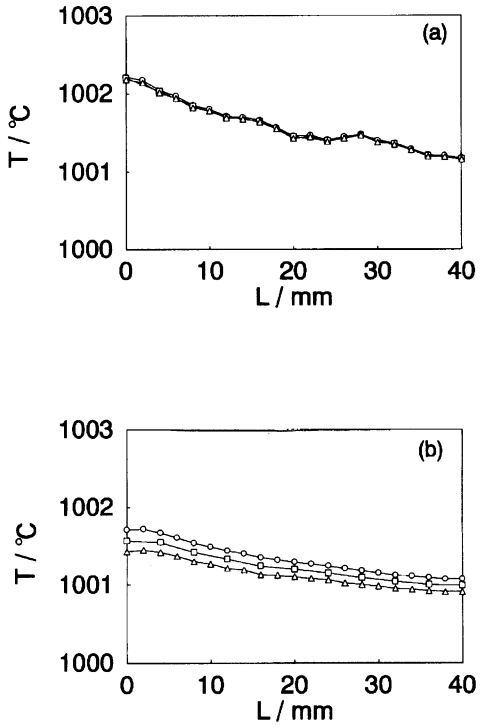

Fig. 7. Temperature distributions in the tubular solid oxide fuel cells ((a): model cell 1, (b): model cell 2) along the Z-axis in the electrolyte region, ○: at the interface between cathode and electrolyte, □: at the center of electrolyte, △: at the interface between anode and electrolyte.

respond to the thermal stresses along the R-axis and Z-axis caused by the cell expansion along the R-axis and Z-axis, respectively. The large σ_{RR} were produced in the cathode region near the entrance of the cell. The large σ_{ZZ} were also observed in whole cathode region. The shearing stress (σ_{RZ}), which is the thermal stress along the Z-axis caused by the cell expansion along the R-axis, was observed in the cathode region near the entrance. These large stresses in the cathode region were caused by the large heat production in cathode and the mismatch between the linear expansion coefficients of yttria-stabilized zirconia electrolyte and porous $LaMnO_3$ cathode.

Figure 10 shows the thermal stress distribution in model cell 2. All stresses were concentrated on the entrance region of cell materials. The tendency of the thermal stress distribution in model cell 2 was different

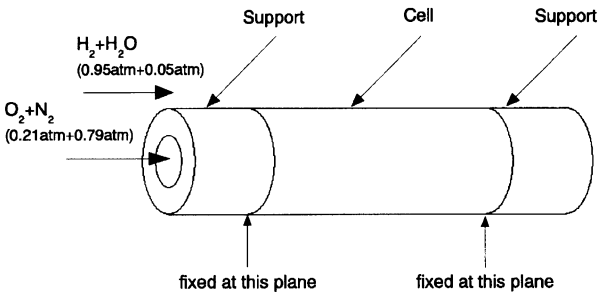

Fig. 8. Boundary conditions for the calculation of thermal stress distribution.

from those in model cell 1. The most interesting feature was the order of thermal stresses in these model cells. The use of hydrogen in model cell 2 was 2% less than those in model cell 1, while the five times thicker elec-

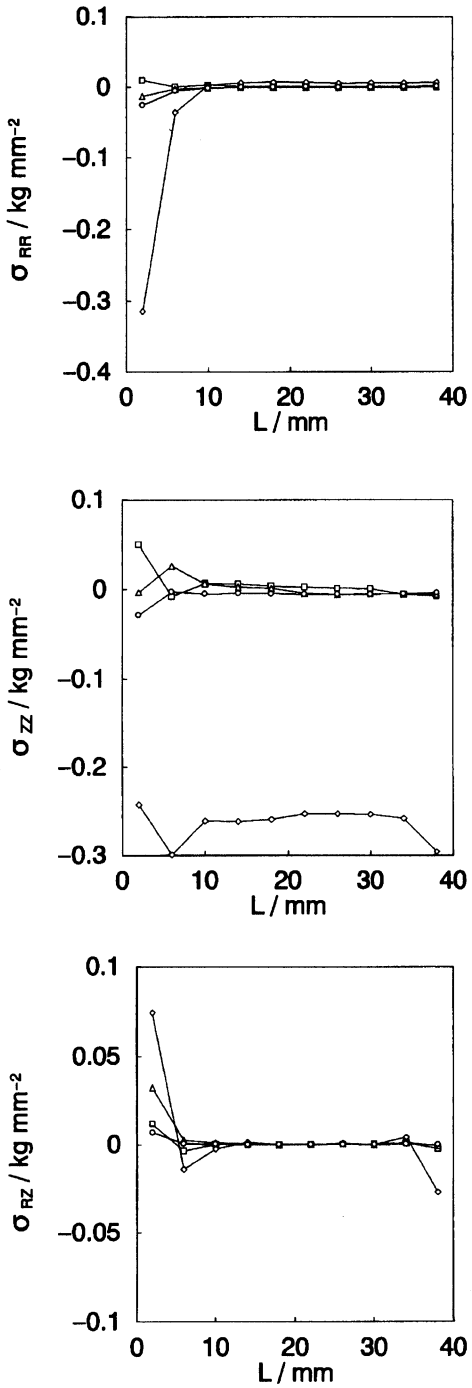

Fig. 9. Thermal stress distributions in the tubular solid oxide fuel cells (model cell 1), principal stress (σ_{RR}), principal stress (σ_{ZZ}), shearing stress (σ_{RZ}), □ : in the substrate, ◇ : in the cathode, △ : in the electrolyte, ○ : in the anode.

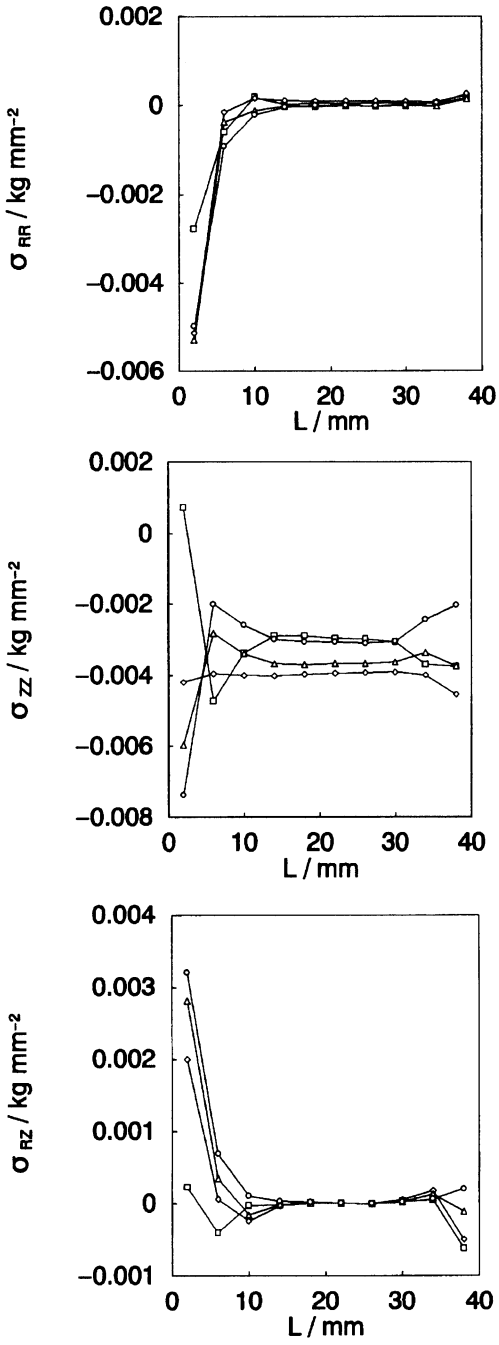

Fig. 10. Thermal stress distributions in the tubular solid oxide fuel cell (Model cell 2), principal stress (σ_{RR}), principal stress (σ_{ZZ}), shearing stress (σ_{RZ}), □ : in the substrate, ◇ : in the cathode, △ : in the electrolyte, ○ : in the anode.

trolyte provides one-fiftieth of the thermal stress. However, larger polarization is produced by the latter, owing to the greater ohmic resistance of the electrolyte. Since the use of hydrogen decreases with increasing thickness of electrolyte, the thickness should be optimized considering both the thermal stability and cell performance.

To realize the tubular SOFC with high energy conversion efficiency and high stability, the thermal expansion coefficients of cell materials have to be adjusted. For example, the linear expansion coefficient of cathode can be changed by the porosity. However, it is difficult for both electrochemical and mechanical parameters to be optimized simultaneously.

Though the conversion efficiency of the electric energy decreases with increasing thickness of electrolyte, the stability of the cell materials increases significantly. The development of the new cell designs and materials is very important in order to make SOFC practical.

References

1) T. Kawada, N. Sakai, H. Yokokawa, and M. Dokiya, *J. Electrochem. Soc.*, **137**, 3042 (1990).
2) H. S. Isaacs and L. J. Olmer, *J. Electrochem. Soc.*, **129**, 436 (1982).
3) F. J. Rohr, "Solid Electrolyte," ed by P. Hagenmuller and W. van Gool, Academic Press, New York (1978), p. 431.
4) G. Wilemski, *J. Electrochem. Soc.*, **130**, 117 (1983).
5) A. Hirano, S. Nakamura, M. Ippommatsu, and K. Ishimaru, *Denki Kagaku*, **58**, 842 (1990).
6) A. Hirano and M. Ippommatsu, private communication.
7) N. J. Maskalick, "Proceedings of The First International Symposium on Solid Oxide Fuel Cell," ed by S. C. Sihghal, Hollywood, Fla. (1990), Vol. 89-11, p. 279.
8) K. Kanamura, S. Yoshioka, and Z. Takehara, *Bull. Chem. Soc. Jpn.*, **64**, 1828 (1991).
9) Z. Takehara, K. Kanamura, and S. Yoshioka, *J. Electrochem. Soc.*, **136**, 2506 (1989).
10) K. Kanamura, S. Yoshioka, and Z. Takehara, *J. Electrochem. Soc.*, **138**, 2165 (1991).
11) W. D. Kingery, H. K. Bowen, and D. R. Uhlman, "Introduction to Ceramics," John Wily & Sons, New York (1976), p. 642.
12) Y. Ohno, S. Nagata, and H. Sato, *Solid State Ionics*, **9 &10**, 979 (1983).